Available online at www.sciencedirect.com
ScienceDirect
Journal of Magnetic Resonance 184 (2007) 337–343
JMR Journal of Magnetic Resonance
www.elsevier.com/locate/jmr

Communication

Multiple echo NMR velocimetry: Fast and localized measurements of steady and pulsatile flows in small channels

L. Guy Raguin [a,1], Luisa Ciobanu [b,*]

[a] Department of Mechanical Engineering, University of Illinois at Urbana-Champaign, IL, USA
[b] Biomedical Imaging Center, Beckman Institute for Advanced Science and Technology, University of Illinois at Urbana-Champaign, IL, USA

Received 8 July 2006; revised 31 October 2006
Available online 16 November 2006

Abstract

The understanding of fluid transport in miniaturized flow devices is an important component in the design of flow cells, micromixers, and microreactors. In this manuscript, we employ NMR in the form of a voxel-selective multiple modulation multiple echo sequence (MMMEV) to monitor average velocities in individual microchannels inside a six-channel network. The technique produces average velocities which are consistent with the imposed flow rates. In addition, we take advantage of the short acquisition time (32 ms per velocity component) of the technique to quantitatively track the time evolution of the fluid velocity in a pulsatile flow phantom.

Keywords: MR velocimetry; Coherence pathways; Field gradient; Phase; Flow rate; Pulsatile flow

1. Introduction

In the last decade, the technology in biomechanical and electro-mechanical devices has become more and more miniaturized, resulting in lab-on-a-chip concepts. At present, the investigation of fluid transport in such miniaturized devices is primarily performed using optical imaging techniques, such as microscopic particle image velocimetry (micro-PIV [1]). These methods require not only optically accessible media (transparent flow cells, mixers or reactors), but also microscopic particles to trace the flow paths. The tracer particles can modify the hydrodynamic properties of the fluid, which can highly impact the flow characteristics, especially at very small length scales.

Nuclear magnetic resonance (NMR) imaging techniques constitute valid alternatives for flow studies given that NMR is non-invasive and compatible with both opaque and transparent media. NMR velocimetry in the form of flow-compensated phase contrast [2], spin tagging imaging [3] or pulsed gradient spin echo (PGSE) [4,5], is an established technique, especially at larger scales. In the microscopic regime, NMR has been used in combination with microfluidic devices for the investigation of reaction kinetics [6,7] and protein conformation changes [8]. Some of the above mentioned MR velocimetry methods, in particular PGSE, have been used to generate flow maps inside microstructures such as flow cells [9] and micromixers [10]. While PGSE results in accurate three-dimensional velocity profiles, it has the drawback of being time-consuming. This method is thus not practical in cases where a fast, robust, non-invasive method is needed to provide quality control and testing of flow cell, reactor, or mixer designs under varying conditions, such as flow rates, temperature, and pressure. Moreover, for this type of testing only the average velocity in individual channels may be required, and therefore, fast and quantitative methods which can provide such information are desirable. Several groups have recently introduced fast methods for flow and diffusion measurements, based on multiple modulation multiple echo

* Corresponding author. Present address: BioImaging Center, Pfizer Global Research and Development, Ann Arbor, MI 48105, USA. Fax: +1 734 622 4398.
E-mail address: luisa.ciobanu@pfizer.com (L. Ciobanu).
[1] Present address: Department of Mechanical Engineering, Michigan State University, East Lansing, MI, USA.

1090-7807/$ - see front matter © 2006 Elsevier Inc. All rights reserved.
doi:10.1016/j.jmr.2006.10.015

(MMME) techniques [11–13]. In the current manuscript, we present a voxel-resolved MMME pulse sequence for velocimetry (MMMEV), and demonstrate its utility by measuring flow in the individual channels of a microchannel network. In addition, we show that this fast method constitutes an accurate technique to quantitatively track unsteady flows by acquiring velocity measurements in a pulsatile flow phantom that match with the imposed flow-through.

2. Method

2.1. Theory

In the presence of a magnetic field gradient **G**, the transverse magnetization accumulates a phase ϕ at time T given by

$$\begin{aligned}\phi(T) &= \gamma \int_0^T q(t)[\mathbf{G}\cdot(\mathbf{v}t+\mathbf{r}_0)+B_0]\,\mathrm{d}t \\ &= \phi_1(T)+\phi_0(T)+\gamma B_0\int_0^T q(t)\,\mathrm{d}t \end{aligned} \quad (1)$$

where B_0 is the static, polarizing magnetic field, and q is the magnetization state ($q=1$ for M_+, $q=-1$ for M_- and $q=0$ for M_0). The initial position and the velocity vectors, $\mathbf{r}_0$ and $\mathbf{v}$, contribute to the phase accumulation via the terms ϕ_0 and ϕ_1, respectively. The times $T=T_j$ for which $\phi_0=0$ correspond to times at which the jth echo appears (an echo forms when previously in-phase magnetization refocuses [14]). Therefore the phase of each echo becomes $\phi(j)=\phi_1(j)$.

We decompose $\phi_1(j)$ as

$$\begin{aligned}\phi_1(j) &= \sum_{i=x,y,z}\phi_{1,i}(j) = \sum_{i=x,y,z}\gamma\int_0^{T_j} q(t)G_i(t)v_i t\,\mathrm{d}t \\ &= \sum_{i=x,y,z} v_i c_{Q,i}(j) \end{aligned} \quad (2)$$

In Eq. (2), v_i and G_i are the velocity and gradient components along the i axis, and $c_{Q,i}(j)$, defined as

$$c_{Q,i}(j) = \gamma\int_0^{T_j} q(t)G_i(t)t\,\mathrm{d}t \quad (3)$$

denotes the sensitivity of the coherence pathway (Q) to the velocity. The coherence pathway formalism Q has been recently described in [15,16].

If the following condition is imposed:

$$c_{Q,i}(j)=0 \quad \text{for } i=x,y \text{ and all echoes } j \quad (4)$$

then Eq. (2) becomes

$$\phi_1(j) = v_z c_{Q,z}(j) \quad (5)$$

It follows that each echo phase $\phi(j)$ is proportional with the z component of the velocity, v_z: $\phi(j)=v_z c_{Q,z}(j)$. The velocity component of interest, v_z, is then experimentally determined as the slope of the measured phase at the jth echo, $\phi_1(j)$, as a function of $c_{Q,z}(j)$. More generally, all three velocity components can be measured individually in three steps, provided that for each velocity component measurement the magnetic gradient $G_i(t)$ is tailored appropriately to impose condition (4) on the other two axes.

2.2. Experiments

All experiments were conducted using a Varian Unity/Inova 600 MHz NMR spectrometer equipped with gradients with a maximum strength of 90 G/cm and a 30 mm diameter RF probe. Pulse programming was performed on Varian VNMR software, and the data were processed and analyzed with MATLAB 6.50 (The MathWorks, Inc.).

The pulse sequence used is shown in Fig. 1; pulse and delay timings are defined in this schematic. The sequence is based on the fact that multiple RF pulses in the presence of a constant gradient generate independently evolving coherence pathways giving rise to multiple echoes [17]. In the present implementation, we use four rectangular RF pulses, which generate 13 echoes. The RF pulse flip angles are $\alpha_1/\alpha_2/\alpha_3/\alpha_4 = 51°/77°/77°/110°$. This set of flip angles was previously determined to result in echoes of similar magnitudes [11]. The phases of the RF pulses are all zero. Magnetic field gradients are applied between, during, and

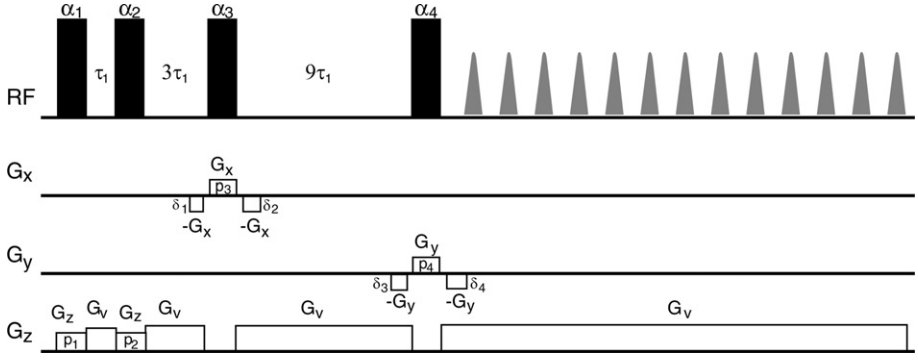

Fig. 1. MMMEV pulse sequence. The four RF pulses generate 13 echoes, each of them containing phase information. The G_v gradient acts as flow-encoding gradient, while G_x, G_y, and G_z select the voxel of interest. The negative gradient pulses are used to null the first order G_x and G_y gradient moments.

Table 1
Coherence pathways for each of the 13 echoes produced by the pulse sequence shown in Fig. 2

Echo index j	q_0	q_1	q_2	q_3	q_4
1	0	1	0	0	−1
2	0	−1	1	0	−1
3	0	0	1	0	−1
4	0	1	1	0	−1
5	0	−1	−1	1	−1
6	0	0	−1	1	−1
7	0	1	−1	1	−1
8	0	−1	0	1	−1
9	0	0	0	1	−1
10	0	1	0	1	−1
11	0	−1	1	1	−1
12	0	0	1	1	−1
13	0	1	1	1	−1

after the pulses. Along the direction of the velocity component of interest (e.g. along the z-direction), a constant field gradient G_v is applied between and after the RF pulses to encode the velocity component.

Gradients along x, y, and z are applied during the RF pulses in order to select only the voxel of interest. In addition, along both x and y directions, refocusing gradient lobes equal in magnitude to G_x and G_y are applied, as shown in Fig. 1. The durations of the refocusing gradients, δ_1, δ_2, δ_3, and δ_4, are calculated such that the condition given by Eq. (4) is satisfied. To do so, each slice-selective gradient is split into halves, since each half corresponds to a different q. Then, for each half there corresponds a refocusing gradient lobe. The duration δ is such that within the segment with the same q that comprises the refocusing gradient lobe and one half of the slice-selective gradient, the first moment of the composite gradient pulse is zero. Pulse sequences to measure the other two velocity components are written by permuting x, y, and z appropriately. For all experiments, the delays between the RF pulses are $\tau_1 = 900\ \mu s$, $\tau_2 = 3\tau_1$, and $\tau_3 = 9\tau_1$, respectively, and all RF pulses are 200 μs long. The resulting durations for the refocusing gradients are: $\delta_1 = 109.972\ \mu s$, $\delta_2 = 110.064\ \mu s$, $\delta_3 = 109.992\ \mu s$, and $\delta_4 = 110.02\ \mu s$. Data points are collected over a period of 20 ms (np = 400, SW = 20 kHz, nt = 1), resulting in a total acquisition time per velocity component of 32 ms.

The coefficients q used in Eq. (3) are shown for each individual echo in Table 1 [11]. Each coherence pathway is characterized by five coefficients, q_0, q_1, q_2, q_3, q_4, where $q_0 = 0$ is the magnetization state before the first pulse, $q_4 = -1$ is the magnetization state during the detection period, and intermediate q_m values correspond to the periods between the mth and $(m+1)$th RF pulses.

2.3. Validation

The pulse sequence is first tested on a simple phantom: a rigid tube (inner diameter 3.175 mm) connected to a syringe pump. The velocity is measured along all three axes,

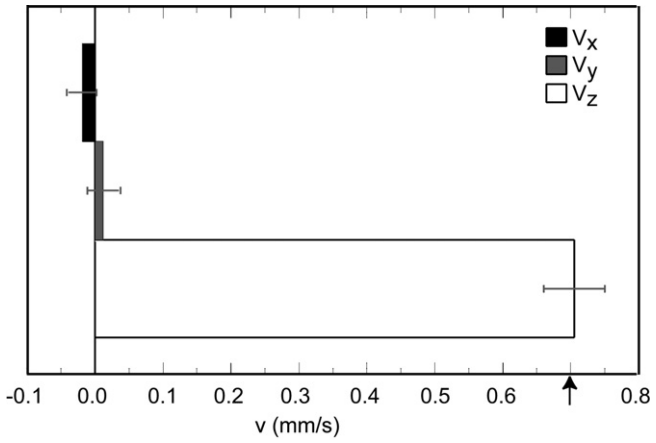

Fig. 2. MMMEV results for velocity measurements in a rigid tube along all three directions. The arrow indicates the predicted v_z velocity corresponding to a flow rate of 20 ml/h. The bars indicate the standard deviation over ten measurements.

for an imposed flow rate of 20 ml/h in a voxel located in the middle of the tube with dimensions of $4 \times 4 \times 2\ mm^3$. The velocity-encoding gradient is $G_v = 10$ G/cm. The results, obtained from ten measurements, are shown in Fig. 2. The measured average velocity along the axis of the tube is found to be 0.705 ± 0.045 mm/s, which is consistent with the predicted velocity of 0.702 mm/s. Along the other two axes, the mean velocity should be zero, which agrees very well with the experimental results. We have thus demonstrated our ability to measure the components of a velocity vector independently by canceling the phase contribution due to the voxel selective gradients along the other two axes.

3. Results and discussion

3.1. Localized velocity measurements inside a microchannel network

A six-microchannel network was built using stereolithography (Fig. 3A). Each channel is 18 mm long with a rectangular cross-section of about $0.615\ mm^2$. The inlet and outlet of the microchannel network are connected to Teflon tubing. The inlet tubing is attached to a syringe pump (Harvard Apparatus, Holliston, MA). Water doped with copper sulfate ($T_1 = 0.25$ s, $T_2 = 0.22$ s) flows in one direction inside three channels and returns through the other three (Fig. 3B). By design, the flow rate in the three left channels is equal to the flow rate in the three right channels, resulting in a zero net flow rate in a cross-section, which allows a quick assessment of the accuracy of the velocity measurements. The flow in individual channels may not be identical due to slight differences in cross-sectional areas and inlet/outlet conditions, which lead to an uneven flow distribution.

A two-dimensional spin echo image is acquired with a nominal in-plane resolution of 50 μm and a slice thickness

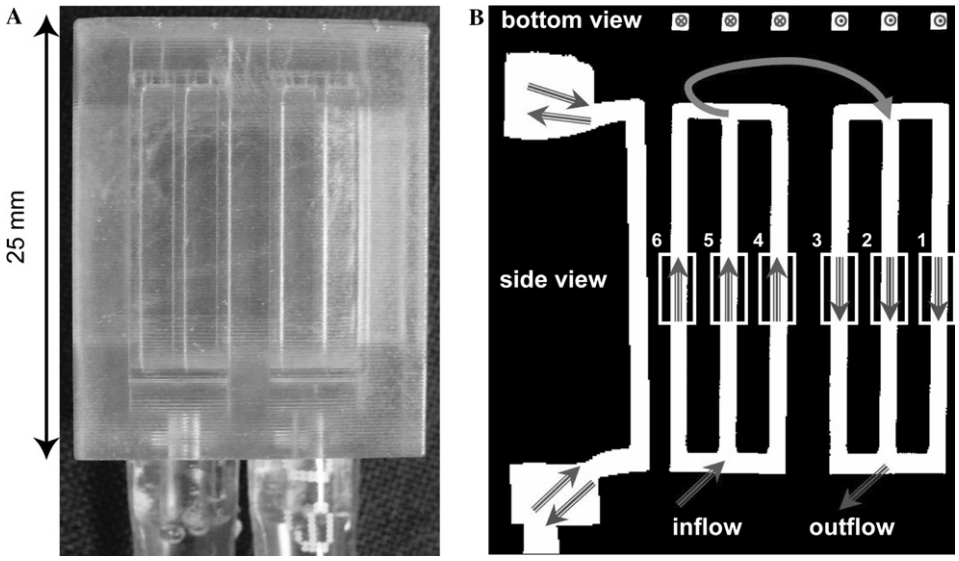

Fig. 3. Stereolithographic resin microchannel network. (A) Digital photograph. The channels have rectangular cross-sections of about 0.615 mm^2 and are 18 mm long. (B) Binarized MRI spin density image obtained using manual threshold showing the flow paths. The image was taken under static conditions; all the channels were filled with water and the syringe pump was stopped. The positions of the voxels in which the velocities are measured are also shown.

of 1.5 mm in order to position the voxels containing the individual microchannels in which the velocity is to be measured. The positions of the selected voxels are indicated in Fig. 3B. The dimensions of the selected voxels are $4 \times 1.5 \times 1.5\ mm^3$. Measurements for flow rates ranging from 2 to 10 ml/h are then performed. The magnitude of the flow-encoding gradient G_v is varied between 6 and 12 G/cm depending on the flow rate (smaller gradients are needed for higher flow rates to avoid phase wrapping).

MMMEV data sets are acquired for each of the six microchannels, first with no flow, and then with flow. The static data sets are used as phase references for the flow measurements. In terms of numerical data processing, for each flow rate we compute the phase differences $\phi_{1,j} = \phi_{1,j,\text{flow}} - \phi_{1,j,\text{static}}$, where $j = \{1, \ldots, 13\}$ is the echo index. The coefficients $c_{Q,z}(j)$ are calculated for each echo using Eq. (3). The times at which the echoes occur are determined experimentally (these times can be calculated theoretically using the formalism developed by Sodickson and Cory [18]). As representative examples of the velocity measurements, in Fig. 4 the phase shift $\phi_1(j)$ is plotted as a function of $c_Q(j)$ for two voxels, corresponding to microchannels #1 and #6, for imposed flow rates of 4, 6, and 8 ml/h. The flow velocities are extracted from the data points as the slope of zero-intercept linear fits. The reference scan is not necessary; however, if a reference scan is not used the data points should be fitted using an unconstrained linear regression (not forced to pass through origin). The intercept of the fit gives the constant phase ϕ_0.

A careful analysis of the pulse sequence shown in Fig. 1 reveals that echoes 1, 11, 12, and 13, which are generated by the first, second, and fourth RF pulses are contaminated by signals coming from spins located outside the voxel of interest. These echo pathways are not affected by the third slice-selective RF pulse (which selects the voxel dimension in the x direction) and contain signals from spins located in the entire zy plane. Therefore these echoes are not used in our velocity analysis. In order to remedy this situation and use all 13 echoes, the RF pulses would need to be replaced with multidimensional spatially selective RF pulses [17,18]. Alternatively, the unwanted echoes can be removed by adequate phase cycling, with the disadvantage that this will require repetitive scans and thus increase the acquisition time.

The results for individual microchannels for all flow rates are presented in Table 2, where the standard deviation is calculated from ten measurements. The cross-sectional area for each channel was measured via a high resolution spin echo image (25 μm in-plane resolution). This allows the computation of the average inflow and outflow velocities, experimental and predicted, which are shown in Table 3. As illustrated by Tables 2 and 3, the average inflow and outflow velocities obtained agree within 8% and match the imposed flow rate within 8%.

3.2. Pulsatile flow measurements

A phantom was constructed out of polyethylene rigid tubing (inner diameter 3.175 mm) in order to preserve the pulsatile flow waveform generated by a programmable Harvard Apparatus pump (Harvard Apparatus, Holliston, MA). The phantom is filled with an aqueous copper sulfate solution ($T_1 = 0.25$ s, $T_2 = 0.22$ s), and placed in the magnet with the flow direction parallel to the direction of the magnetic field. The flow rate is varied according to an imposed triangular waveform with a peak flow rate of 60 ml/h. The velocity-encoding gradient is $G_v = 4$ G/cm. The velocity is measured every 2 s in a voxel with dimensions of $4 \times 4 \times 2\ mm^3$. The sampling rate is limited by the performance of the pump and ultimately by T_1 relaxation effects.

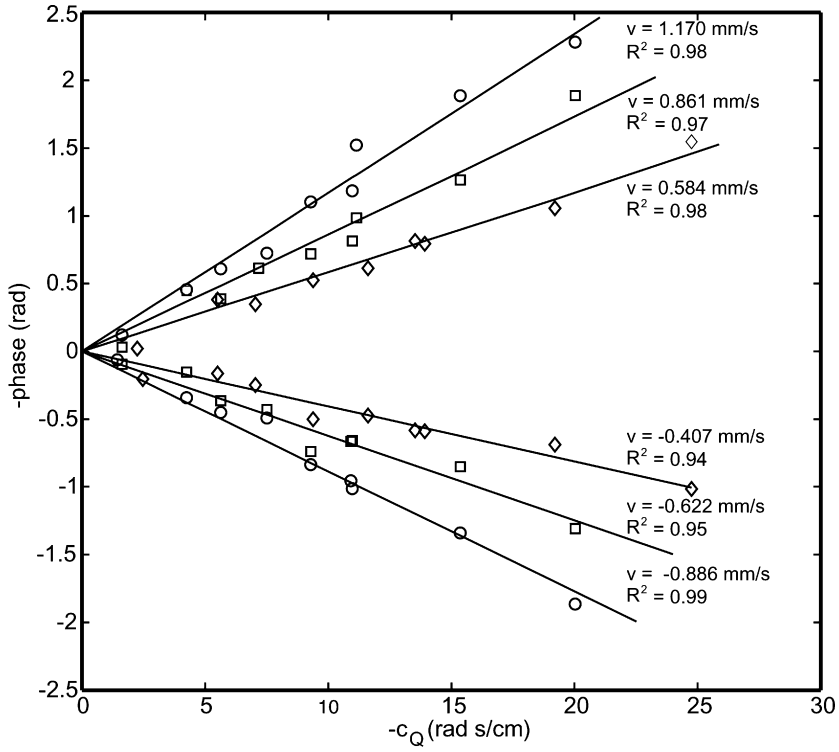

Fig. 4. Flow-induced phase shift versus c_Q for three different flow rates in microchannels #1 (negative velocities) and #6 (positive velocities). The data points for each flow rate were fitted with straight lines, the slopes giving the corresponding mean flow velocities. Symbols: ○ 8 ml/min, □ 6 ml/min, ◇ 4 ml/min.

Table 2
The average velocities in each individual channel

Channel	Velocity (mm/s)				
	10 ml/h	8 ml/h	6 ml/h	4 ml/h	2 ml/h
1	-1.08 ± 0.06	-0.88 ± 0.07	-0.60 ± 0.03	-0.39 ± 0.03	-0.18 ± 0.02
2	-1.41 ± 0.08	-1.14 ± 0.03	-0.90 ± 0.04	-0.68 ± 0.04	-0.35 ± 0.02
3	-1.64 ± 0.04	-1.35 ± 0.08	-1.00 ± 0.03	-0.67 ± 0.02	-0.34 ± 0.02
4	1.46 ± 0.04	1.19 ± 0.06	0.95 ± 0.04	0.68 ± 0.04	0.36 ± 0.03
5	1.57 ± 0.09	1.32 ± 0.11	0.83 ± 0.05	0.51 ± 0.03	0.27 ± 0.02
6	1.53 ± 0.05	1.21 ± 0.05	0.90 ± 0.04	0.57 ± 0.04	0.28 ± 0.05

The values are obtained from ten measurements.

Table 3
Comparison of experimental and predicted average inflow and outflow velocities

Q (ml/h)	Average velocity (mm/s)			
	Experimental		Predicted	
	Inflow	Outflow	Inflow	Outflow
10	1.52 ± 0.04	-1.38 ± 0.04	1.520	−1.491
8	1.24 ± 0.06	-1.12 ± 0.03	1.216	−1.193
6	0.89 ± 0.03	-0.83 ± 0.03	0.912	−0.895
4	0.59 ± 0.02	-0.58 ± 0.03	0.608	−0.597
2	0.32 ± 0.02	-0.29 ± 0.02	0.304	−0.298

For the pulsatile flow experiment, we chose the last measurement as a reference, which corresponds to static conditions. The comparison between the experimentally measured velocities and the waveform imposed is shown in Fig. 5. The experimentally derived velocities agree well with the imposed flow rates in both magnitude and timing: the overall root-mean-square (rms) of the difference between the measured and analytical velocities is 0.168 mm/s, corresponding to 8% of the peak fluid velocity.

4. Conclusion

In this manuscript, we employ NMR in the form of a voxel selective multiple modulation multiple echo sequence (MMMEV) to monitor average velocities in individual microchannels inside a six channel network and inside a pulsatile flow phantom. With acquisition times of several tens of milliseconds, the technique produces average velocities that are consistent with the imposed flow rates and

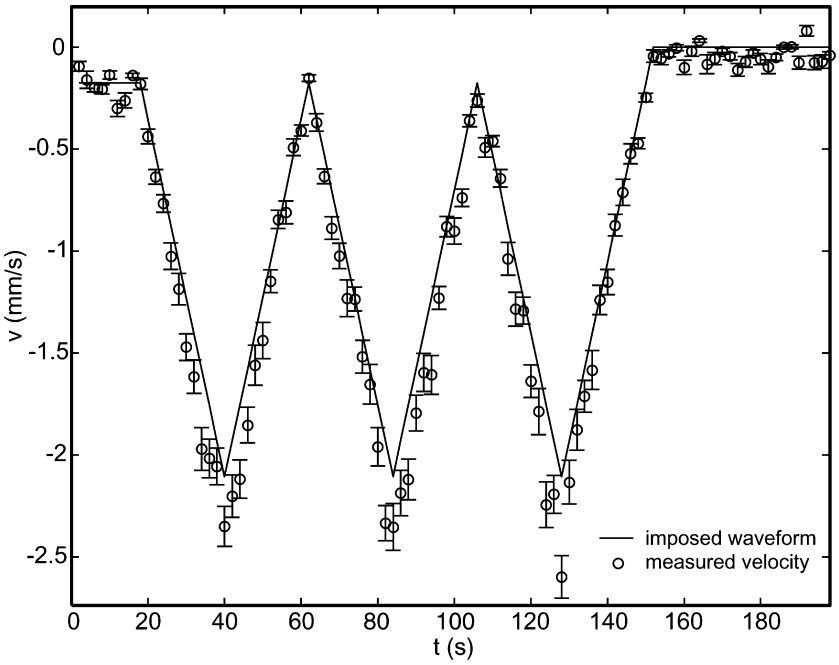

Fig. 5. Comparison of the velocity measured by MMMEV with the imposed waveform in a pulsatile flow experiment. The solid line represents the imposed waveform. Open circles are experimental data points and the error bars correspond to the statistical uncertainty in the slope measurement from the linear fit of the echo phases versus $c_{Q,z}$.

measured cross-sectional areas, both in steady and pulsatile regimes. The size of the voxel in which the velocity can be measured is limited by the maximum magnetic field gradient available and ultimately by adequate signal-to-noise ratio.

This technique can be used to provide quality control and testing of flow cells, microreactors, or micromixers under varying conditions, such as flow rates, temperature, and pressure fields. Thanks to the ability to provide localized velocity information in nearly real time, the presented flow measurement technique could be very useful in a variety of biomedical applications. For example, it can be used for the assessment of different pathological conditions (cerebrovascular abnormalities, coronary artery disease), during intravascular procedures, or for studies of vascular hemodynamics *in vivo*. The implementation of the technique is simple and requires standard MR imaging hardware. The success of the method for velocity measurements is limited by factors such as: proper setting of the velocity sensitivity, proper alignment of the flow-encoding gradient with the axis of blood flow, and good selection of the voxel of interest (in cases where blood vessels are close to each other, it may not be possible to select only the vessel of interest, resulting in average velocity measurements that may not be easily interpreted).

Acknowledgments

This work was supported by the Biomedical Imaging Center, Beckman Institute for Advanced Science and Technology, the Richard W. Kritzer Foundation, and the NSF Science and Technology Center of Advanced Materials for Purification of Water with Systems (WaterCAMPWS, Grant CTS-0120978). The authors thank Prof. John Georgiadis for providing the multichannel network. The authors also thank Dr. Yi-Qiao Song for helpful discussions.

References

[1] J.G. Santiago et al., A particle image velocimetry system for microfluidics, Exp. Fluids 25 (1998) 316.
[2] K.W. Moser et al., Velocity measurements of flow through a step stenosis using magnetic resonance imaging, Exp. Fluids 29 (2000) 438.
[3] T.J. Mosher, M.B. Smith, A dante tagging sequence for the evaluation of translational sample motion, Magn. Reson. Med. 15 (1990) 334.
[4] J.D. Seymour, B. Manz, P.T. Callaghan, Pulsed gradient spin echo NMR measurements of hydrodynamic instabilities with coherent structure: Taylor vortices, Phys. Fluids 11 (5) (1999) 1104.
[5] Y. Xia, P.T. Callaghan, K. Jeffrey, Imaging velocity profiles: flow through an abrupt contraction and expansion, AICHE J. 38 (1992) 1408.
[6] L. Ciobanu et al., Measuring reaction kinetics by using microcoil NMR spectroscopy, Angew. Chem. Int. Edit. 42 (38) (2003) 4669.
[7] H. Wensink et al., Measuring reaction kinetics in a lab-on-a-chip by microcoil NMR, Lab Chip 5 (2005) 280.
[8] M. Kakuta et al., Micromixer-based time-resolved NMR: applications to ubiquitin protein conformation, Anal. Chem. 75 (4) (2003) 956.
[9] X. Zhang, A.G. Webb, Magnetic resonance microimaging and numerical simulations of velocity fields inside flowcells for coupled NMR microseparations, Anal. Chem. 77 (2005) 1338.
[10] S. Ahola et al., Monitoring of fluid motion in a micromixer by dynamic NMR microscopy, Lab Chip 6 (2006) 90.
[11] Y.-Q. Song, X. Tang, A one-shot method for measurement of diffusion, J. Magn. Reson. 170 (2004) 136.

[12] Y.-Q. Song, U.M. Scheven, An NMR technique for rapid measurement of flow, J. Magn. Reson. 172 (2005) 31.
[13] E.E. Sigmund, Y.-Q. Song, Multiple echo diffusion tensor acquisition technique, Mag. Reson. Imaging 24 (2006) 7.
[14] E. Jensen, General theory of spin-echoes for any combination of any number of pulses, Acta Polytech. Scand. Phys. Incl. Nucleon. Ser. 7 (1960) 1.
[15] M.D. Hurlimann, Diffusion and relaxation effects in general stray field NMR experiments, J. Magn. Reson. 148 (2001) 367.
[16] Y.-Q. Song, Categories of coherence pathways in the CPMG sequences, J. Magn. Reson. 157 (2002) 82.
[17] R.J. Nelson et al., Counting echoes: application of a complete reciprocal-space description of NMR spin dynamics, Concept Magn. Reson. 10 (1998) 331.
[18] A. Sodickson, D.G. Cory, A generalized *k*-space formalism for treating the spatial aspects of a variety of NMR experiments, Prog. Nucl. Magn. Reson. Spectrosc. 33 (1998) 77.